UC Davis

UC Davis Previously Published Works

Title

Pharmacological Inhibition of mTOR Kinase Reverses Right Ventricle Remodeling and Improves Right Ventricle Structure and Function in Rats

Permalink

https://escholarship.org/uc/item/9488n06c

Journal

American Journal of Respiratory Cell and Molecular Biology, 57(5)

ISSN

1044-1549

Authors

Pena, Andressa
Kobir, Ahasanul
Goncharov, Dmitry
et al.

Publication Date

2017-11-01

DOI

10.1165/rcmb.2016-0364oc

Peer reviewed

eScholarship.org Powered by the California Digital Library
University of California

ORIGINAL RESEARCH

Pharmacological Inhibition of mTOR Kinase Reverses Right Ventricle Remodeling and Improves Right Ventricle Structure and Function in Rats

Andressa Pena[1]*, Ahasanul Kobir[1]*, Dmitry Goncharov[1], Akiko Goda[2], Tatiana V. Kudryashova[1], Arnab Ray[1], Rebecca Vanderpool[3], Jeffrey Baust[1], Baojun Chang[1], Ana L. Mora[1,4], John Gorcsan III[1,2], and Elena A. Goncharova[1,4,5]

[1]Pittsburgh Heart, Lung, and Blood Vascular Medicine Institute, [2]Division of Cardiology, [4]Division of Pulmonary, Allergy, and Critical Care Medicine, Department of Medicine, and [5]Department of Bioengineering, University of Pittsburgh, Pittsburgh, Pennsylvania; and [3]Department of Medicine, University of Arizona, Tuscon, Arizona

ORCID IDs: 0000-0002-2843-5554 (T.V.K.); 0000-0001-7118-6752 (E.A.G.).

Abstract

Pulmonary arterial hypertension (PAH) is characterized by pulmonary vascular remodeling, increased pulmonary artery (PA) pressure, right-heart afterload and death. Mechanistic target of rapamycin (mTOR) promotes smooth muscle cell proliferation, survival, and pulmonary vascular remodeling via two functionally distinct mTOR complexes (mTORCs)-1 (supports cell growth) and -2 (promotes cell survival), and dual mTORC1/mTORC2 inhibition selectively induces pulmonary arterial hypertension PA vascular smooth muscle cell apoptosis and reverses pulmonary vascular remodeling. The consequences of mTOR inhibition on right ventricle (RV) morphology and function are not known. Using SU5416/hypoxia rat model of pulmonary hypertension (PH), we report that, in contrast to activation of both mTORC1 and mTORC2 pathways in small remodeled PAs, RV tissues had predominant up-regulation of mTORC1 signaling accompanied by cardiomyocyte and RV hypertrophy, increased RV wall thickness, RV/left ventricle end-diastolic area ratio, RV contractility and afterload (arterial elastance), and shorter RV acceleration time compared with controls. Treatment with mTOR kinase inhibitor, PP242, at Weeks 6–8 after PH induction suppressed both mTORC1 and mTORC2 in small PAs, but only mTORC1 signaling in RV, preserving basal mTORC2–Akt levels. Vehicle-treated rats showed further PH and RV worsening and profound RV fibrosis. PP242 reversed pulmonary vascular remodeling and prevented neointimal occlusion of small PAs, significantly reduced PA pressure and pulmonary vascular resistance, reversed cardiomyocyte hypertrophy and RV remodeling, improved max RV contractility, arterial elastance, and RV acceleration time, and prevented development of RV fibrosis. Collectively, these data show a predominant role of mTORC1 versus mTORC2 in RV pathology, and suggest potential attractiveness of mTOR inhibition to simultaneously target pulmonary vascular remodeling and RV dysfunction in established PH.

Keywords: mechanistic target of rapamycin complex 1; mechanistic target of rapamycin complex 2; right ventricle; mechanistic target of rapamycin kinase inhibitor; pulmonary hypertension

Pulmonary arterial hypertension (PAH) is a progressive disease with high mortality rates and limited treatment options. Remodeling of small pulmonary arteries (PAs) due to increased proliferation and impaired apoptosis of resident vascular cells is a key feature of PAH that highly contributes to elevated PA pressure (PAP), right ventricle (RV) afterload, and death from heart failure (1, 2). Currently approved therapies do not reverse established pulmonary vascular remodeling,

(Received in original form November 10, 2016; accepted in final form June 26, 2017)

*These authors contributed equally to this work.

This work was supported by National Institutes of Health (NIH)/NHLBI R01HL113178 (E.A.G.), NIH/NHLBI P01HL103455 (A.L.M. and E.A.G.), University of Pittsburgh Heart and Vascular Institute/Pittsburgh Heart, Lung, and Blood Vascular Medicine Institute innovator award (J.G. and E.A.G.); the Pulmonary Hypertension Breakthrough Initiative is supported by NIH R24HL123767-04.

Author Contributions: Conception and design—D.G., A.L.M., J.G., and E.A.G.; experimental work—A.P., D.G., A.G., T.V.K., A.R., R.V., J.B., and B.C.; analysis—A.P., A.K., D.G., A.G., A.R., R.V., B.C., J.G., and E.A.G.; interpretation— D.G., A.G., R.V., A.L.M., J.G., and E.A.G.; drafting the manuscript—A.P., A.K., and E.A.G.; intellectual content—D.G., A.G., J.G., and E.A.G.

Correspondence and requests for reprints should be addressed to Elena A. Goncharova, Ph.D., Biomedical Science Tower, Room E1259, 200 Lothrop Street, Pittsburgh, PA 15261. E-mail: eag59@pitt.edu

This article has an online supplement, which is accessible from this issue's table of contents at www.atsjournals.org

Am J Respir Cell Mol Biol Vol 57, Iss 5, pp 615–625, Nov 2017
Copyright © 2017 by the American Thoracic Society
Originally Published in Press as DOI: 10.1165/rcmb.2016-0364OC on July 5, 2017
Internet address: www.atsjournals.org

Clinical Relevance

Pulmonary arterial hypertension (PAH) is characterized by pulmonary vascular remodeling, increased pulmonary artery pressure, and right ventricle (RV) dysfunction. Recent studies have demonstrated that up-regulation of mechanistic target of rapamycin (mTOR) complex (mTORC) 1 (which promotes cell growth) and mTORC2 (which supports apoptosis resistance) in PAH pulmonary vasculature promotes vascular smooth muscle remodeling, but the status of mTORCs in PA RV and consequences of dual mTORC1/2 inhibition on RV morphology and function and overall pulmonary hypertension (PH) are not known. In this study, we show that there is predominant up-regulation of mTORC1 compared with mTORC2 in RV in experimental PH, provide the link between mTORC1 activation and RV cardiomyocyte hypertrophy, and demonstrate that inhibition of mTOR kinase activity reverses pulmonary vascular remodeling, reduces established PH, and improves RV morphology and functional outcomes. These findings suggest potential attractiveness of mTOR kinase inhibitors to simultaneously target pulmonary vascular remodeling and RV dysfunction.

and development of remodeling-targeting antiproliferative proapoptotic therapeutic strategies is an area of unmet and great need (3). Antiapoptotic signaling pathways, however, often play an important role in normal heart function via supporting cardiomyocyte survival, and cardiovascular complications is one of the common side effects of cytotoxic therapies in cancer survivors (4). It is now clear that the status of RV might be considered as an important part of preclinical testing of remodeling-focused strategies, with an overall goal to identify therapeutic compound(s) that simultaneously reverse established pulmonary vascular remodeling and doesn't worsen or, ideally, improve RV morphology and function.

Mechanistic (formerly "mammalian") target of rapamycin (mTOR) is a master regulator of cell growth, proliferation, and survival (5). mTOR forms a catalytic core of two functionally distinct complexes: mTOR complex (mTORC) 1, a positive regulator of p70 S6 kinase (S6K1)/ribosomal protein S6 signaling and cell growth, and mTORC2, an activator of proproliferative/prosurvival protein kinase Akt (5, 6). Pulmonary artery (PA) vascular smooth muscle (VSM) cell (PAVSMC)–specific activation of mTORC1–S6K1 and mTORC2–Akt in human PAH and experimental pulmonary hypertension (PH) have been reported by several groups, including ours (7–10). We also found that mTORC2 activation in human PAH PAVSMC is required for increased energy generation, cell survival, and activation of mTORC1, which promotes cell proliferation (7–9). Pharmacological inhibition of mTOR kinase activity (which suppresses both mTORC1 and mTORC2 pathways) with small ATP–competitive inhibitor, PP242, improves the metabolomic profile of microvascular PAVSMC from subjects with PAH (11), selectively reduces proliferation, and promotes apoptosis in human PAH, but does not control PAVSMCs, and reverses hypoxia-induced pulmonary vascular remodeling in rats (7), suggestive of potential attractiveness of mTOR kinase inhibitors as a remodeling-focused therapeutic strategy. The status of mTOR signaling in RV during PH progression, however, is not known, and the effects of pharmacological inhibition of mTOR kinase on established PH and RV morphology and function have not been evaluated.

In this study, we aimed to determine the status of mTOR complexes in the PH heart and evaluate effects of pharmacological inhibition of mTOR kinase on established PH and RV structure and function using an SU5416/hypoxia (SuHx) model of severe experimental PH. We found that there are different patterns of mTORC1 and mTORC2 activation in PH pulmonary vasculature and RV. We also report that, in a rat SuHx model of PH, mTOR kinase inhibitor, PP242, suppresses mTORC1–S6 and mTORC2–Akt pathways in small PAs, but only mTORC1–S6 signaling in RV, without affecting basal mTORC2–Akt activity. Finally, we demonstrate that PP242 reverses both pulmonary vascular and RV remodeling and established PH, improves RV morphology and functional parameters and prevents development of RV fibrosis. These data suggest potential attractiveness of this therapeutic strategy to simultaneously target established pulmonary vascular remodeling and RV dysfunction.

Materials and Methods

Animals

All animal procedures were performed under the protocols approved by the University of Pittsburgh (Pittsburgh, PA) Animal Care and Use Committee.

SuHx model of PH. Male Sprague-Dawley rats (6–8 wk old; Charles River Laboratories, Taconic Biosciences, Inc., Hudson, NY) were randomly assigned to five groups (*see* Figure E1 in the online supplement for experimental design). Rats from groups 1, 2, and 4 were injected subcutaneously with vascular endothelial growth factor receptor inhibitor, SU5416 (20 mg/kg; Sigma-Aldrich, St. Louis, MO) followed by 3 weeks of exposure to normobaric hypoxia (10% O_2) and 2 weeks of normoxia (12, 13). For long-term PP242 treatment, 5 weeks after SU5416 injection, rats were subjected to terminal hemodynamic analysis (group 4), or treated with vehicle or PP242 (20 mg/kg, intraperitoneal injection, 5 d/wk) for the next 3 weeks (groups 1 and 2, respectively) (Figure E1). Controls (groups 3 and 5) included same-age male rats maintained under normoxia (12, 13) (Figure E1). Rats from PP242-treated, vehicle-treated, and the appropriate control group were subjected to repetitive noninvasive echocardiography at Day 0 (baseline) and 3, 5, and 8 weeks of experiment (groups 1, 2, and 3; Figure E1). For this, rats were anesthetized with 2.0% isoflurane in a 1:1 O_2/air mixture, and noninvasive echocardiography was performed using the VisualSonics VEVO-770 imaging system with a 12–38 MHz transducer (VisualSonics Inc., Toronto, ON, Canada). Echocardiographic variables included left ventricle (LV) and RV wall thickness (WT), LV dimensions, and calculated volumes for ejection fraction, and LV and RV end-diastolic areas (EDAs) from midventricular short-axis views. After the last echo measurements, terminal hemodynamic analysis was performed (described subsequently here). Upon the completion of data acquisition, lung and

heart tissues were collected from dead animals for morphological and histochemical analysis. Hearts were separated to RV and LV plus septum (S), and Fulton index was calculated as a RV/(LV + S) ratio. For short-term PP242 treatment (*see* Figure E2 for schematic representation of the experiment), PP242 or vehicle were administrated to rats with SuHx-induced PH at Days 54–56 after PH initiation followed by terminal hemodynamic analysis and heart tissue collection.

Chronic hypoxia model of PH. Male Sprague-Dawley rats (6–8 wk old; Charles River Laboratories, Taconic Biosciences, Inc.) were randomly assigned to two groups and exposed for 3 weeks to normobaric hypoxia (10% O_2; hypoxia model of PH [HPH] group) or normoxia (control group). Animals were then subjected to hemodynamic analysis, as described subsequently here, and heart tissues were collected for analysis. Fulton index was calculated as an RV/(LV + S) ratio.

Terminal hemodynamic analysis. Terminal hemodynamic analysis was performed as described previously (13). Briefly, animals were anesthetized with isoflurane (5% for induction, 2% during surgery, and 1% while performing pressure–volume [PV] loop measurements) and *in vivo* PV loop measurements of RV function were performed by a PV catheter. A four-electrode PV catheter (Scisense, Inc., London, ON, Canada) attached to the data acquisition system (EMKA Instruments, Falls Church, VA) was inserted into the apex of the RV. The data were acquired using the EMKA data acquisition boxes and software (AD Instruments, Colorado Springs, CO). After ventricular assessment of PV loop relationships, a 20-mHz Doppler probe was placed over the PA and then over the aortic arch to assess CO and Doppler waveforms (DSPW; Indus Instruments, Houston, TX).

Morphological, immunohistochemical and immunoblot analyses. Morphological, immunohistochemical, and immunoblot analyses were performed as described previously (7, 9, 13). Briefly, lung and RV tissues were fixed in 4% paraformaldehyde solution in PBS overnight, embedded in paraffin, sectioned, and hematoxylin and eosin staining was performed as described previously (9, 13). Images were taken using Olympus Fluoview 1,000 confocal microscope (Olympus, Center Valley, PA); blinded analysis of medial WT of small PAs (25–150 μm outer diameter; minimum of 5 rats/group, minimum of 10 PAs/rat) and RV cardiomyocyte cross-sectional area (minimum of 5 rats/group, minimum of

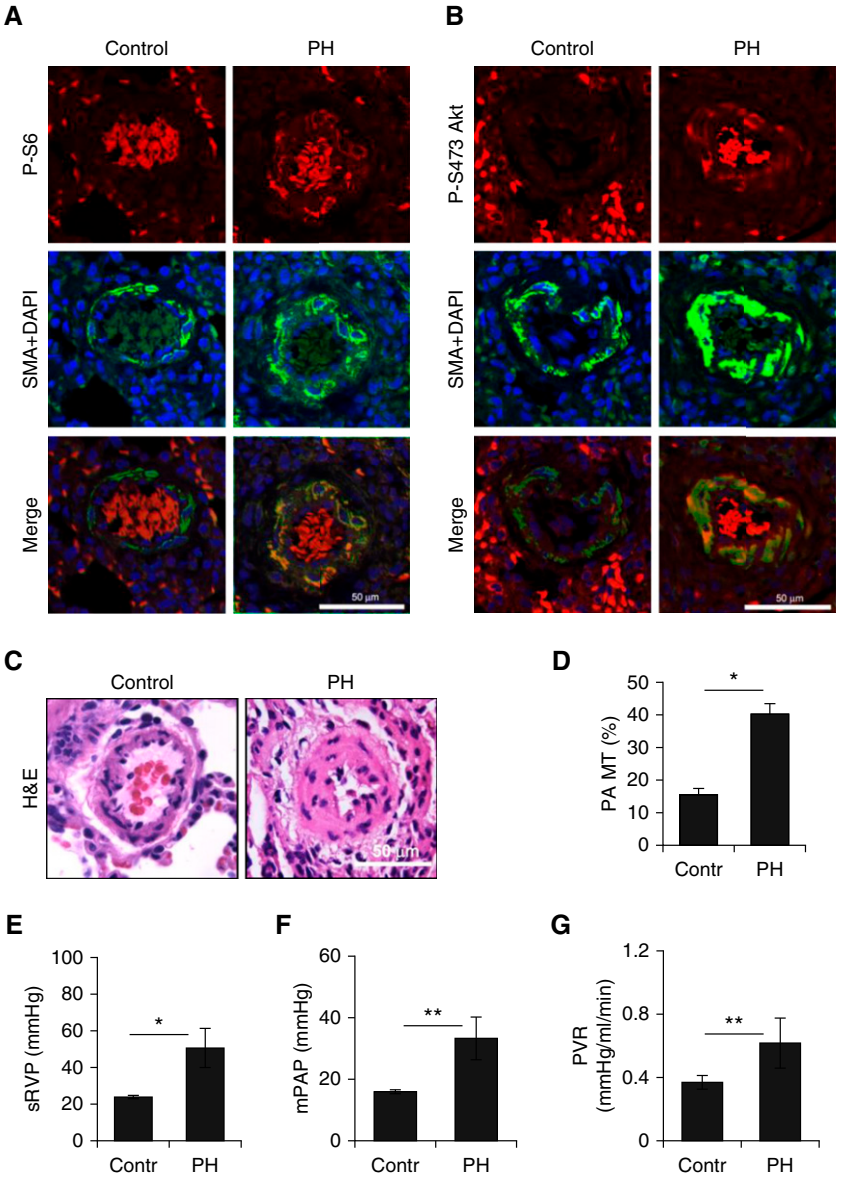

Figure 1. Pulmonary artery (PA) vascular smooth muscle cell–specific mechanistic target of rapamycin (mTOR) complex (mTORC) 1–S6 and mTORC2–Akt activation, pulmonary vascular remodeling, and pulmonary hypertension (PH) in SU5416/hypoxia (SuHx)–exposed rats. (*A* and *B*) Immunohistochemical analysis of lung tissues from male Sprague-Dawley rats with SuHx-induced PH (5 wk after induction) and age-matched controls to detect P-S6 (*red*, *A*), P-Akt (*red*, *B*), smooth muscle actin (SMA; *green*) and 4′,6-diamidino-2-phenylindole (DAPI; *blue*). *Yellow*: SMA (*green*) and P-S6 (*red*) or P-Akt (*red*, *B*) overlap. Images are representative of 3 animals per condition, minimum of 10 vessels per animal. *Scale bars*: 50 μm. (*C* and *D*) PA medial thickness (PA MT) analysis of rats with SuHx-induced PH (5 wk after PH induction) and age-matched controls. Representative images of hematoxylin and eosin (H&E)–stained PAs (*C*) and PA MT analysis (*D*). *Scale bar*: 50 μm; $n = 5$–6 animals/group; minimum of 10 PAs/animal. Data are means ± SE; $^*P < 0.01$. (*E*–*G*) Right ventricular (RV) systolic pressure (sRVP) (*E*), mean pulmonary arterial pressure (mPAP) (*F*), and pulmonary vascular resistance (PVR) (*G*) of rats with SuHx-induced PH (5 wk after induction) and age-matched controls. Data are means ± SE; $n = 5$–6 animals/group; $^*P < 0.01$, $^{**}P < 0.05$. Contr, control; P-S6, phospho-S6.

60 cardiomyocytes/rat) were performed as described in References 13 and 14, respectively. Lung tissue sections were immunostained with anti–P-S6 and anti–P-S473 Akt (Cell Signaling Technology, Beverly, MA). Costaining with anti–α-smooth muscle actin (SMA) antibodies (Sigma-Aldrich) and 4′,6-diamidino-2-phenylindole was performed to detect smooth muscle and cell nuclei, respectively. Immunostaining with anti–von Willebrand factor (vWF) antibody was performed as described in References 15 and 16. RV tissue sections were subjected to Masson's trichrome staining using Masson's Trichrome Stain Kit (Polysciences, Inc., Warrington, PA) as described in Reference 17. Immunoblot analysis of heart tissues, snap frozen in liquid nitrogen, was performed as described previously (7, 13). Anti–P-S6, anti–total S6, anti–P-S473 Akt, anti–total Akt, anti–P-Thr37/46 eIF4E-binding protein 1 (4EBP1), anti-4EBP1, anti–P-serum, glucocorticoid activated kinase 1 (SGK1), anti-SGK1, and anti-tubulin antibodies were purchased from Cell Signaling Technology; anti–collagen I-A and anti-vWF antibodies were purchased from Abcam (Cambridge, MA).

Cell cultures. Distal (type III) PA endothelial cells (PAECs) from nondiseased (control) subjects and patients with PAH were provided by the PHBI (Pulmonary Hypertension Breakthrough Initiative) and University of Pittsburgh Vascular Medicine Institute Cell Processing Core under protocols approved by PHBI and the University of Pittsburgh institutional review boards. Primary (4–8 passages) PAECs from three control and four PAH subjects were used in each experiment. Cells were cultured in specialized complete media with endothelial cell growth supplement and 2% FBS (Lonza Walkersville, Inc., Walkerscille, MD) (18). Cell growth experiments were performed as described in References 7, 13, 18. Briefly, cells were plated into 12-well plates (100,000 cells/well) in triplicates for each time point and cultured in complete media supplemented with 2% FBS. At 24 hours after plating, media were replaced with complete media supplemented with 2% FBS with or without 0.01, 0.1, 1, or 10 μM PP242 or diluent. At 24, 48, and 72 hours after media replacement (Days 1, 2, and 3, respectively), the cells were counted using Countess II FL Automated Cell Counter (Thermo Fisher Scientific, Waltham, MA). Three independent measurements, each in duplicate, were performed per cell culture for each experimental point. Immunoblot analysis to detect P-S6, S6, P-S473 Akt, and Akt was performed at the 72-hours time point, as described in References 7 and 13.

Statistical Analysis

Immunoblots were analyzed using ImageJ and StatView (SAS [Statistical Analysis System], Cary, NC) software, hemodynamic and morphometric data using Indus Instruments, IOX2 (Emka Technologies, Falls Church, VA), Emka (Emka Technologies), Matlab (MathWorks, Natick, MA), and Image J (National Institutes of Health, Bethesda, MD). Statistical comparisons between two groups were performed by the Mann-Whitney *U* test. Statistical significance was defined as a *P* value of 0.05 or less.

Results

PAVSM-Specific Activation of mTORC1–S6 and mTORC2–Akt in Pulmonary Vasculature of Rats with SuHx-Induced PH

Immunohistochemical analysis of lung tissue from rats with SuHx-induced PH 5 weeks after induction and age-matched controls (Figure E1, groups 4 and 5) showed that PH rats have marked increase of mTORC1-specific P-S6 and mTORC2-specific P-S473 Akt, molecular signatures

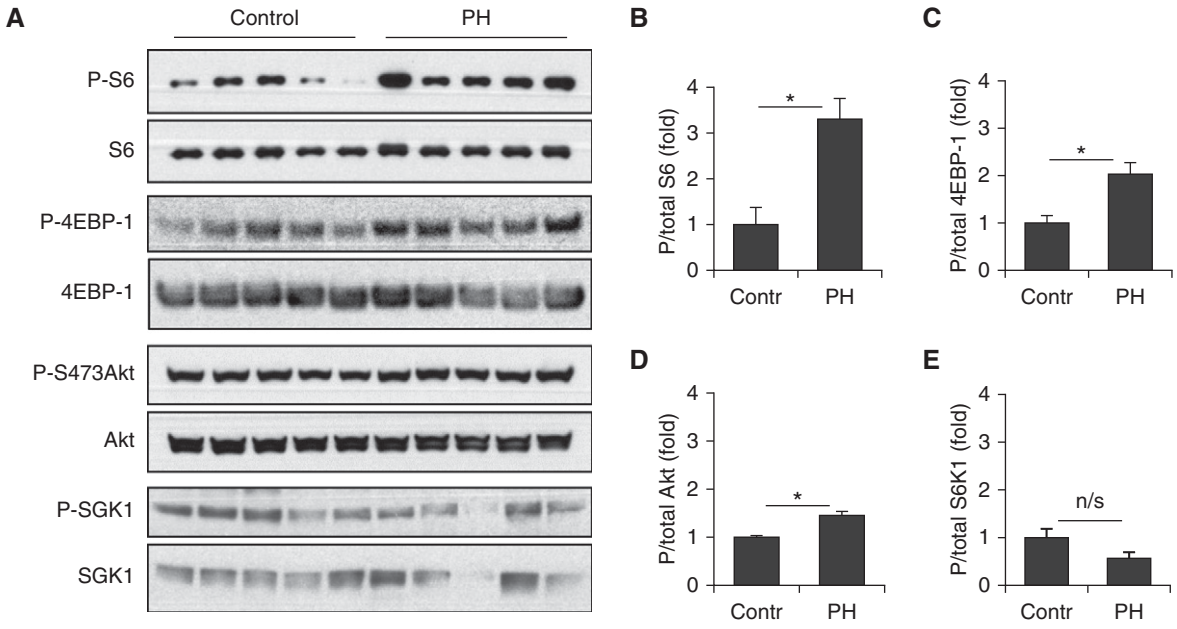

Figure 2. Predominant up-regulation of mTORC1 signaling in RV from rats with SuHx-induced PH. (*A*) Immunoblot analysis of RV tissues from rats with SuHx-induced PH (5 wk after induction) and age-matched controls to detect indicated proteins. (*B–E*) Data represent fold change in Phospho:total protein ratio to control. Data are means ± SE; $n = 5$ rats/group; $^*P < 0.01$. 4EBP1, eucaryotic initiation factor 4E-binding protein 1; n/s, nonsignificant; P-4EBP-1, phospho-4EBP1; P-S473Akt, phospho-serine 473 Akt; P-SGK1, phospho SGK1; SGK1, serum and glucocorticoid-regulated kinase.

of mTORC1 and mTORC2 activation, respectively (6, 7), in SMA-positive areas of small (25–150 μm) remodeled PAs (Figures 1A and 1B) corroborating previous findings on human PAH and experimental PH (7–10). Animals from the PH group had significant increases in PA medial thickness (Figures 1C and 1D), elevated RV systolic pressure (sRVP), mean PAP (mPAP), and pulmonary vascular resistance (PVR) (Figures 1E–1G). These data show that, 5 weeks after PH induction, SuHx-exposed rats develop significant pulmonary vascular remodeling and PH that is associated with PAVSM-specific activation of mTORC1–S6 and mTORC2–Akt signaling pathways.

Impaired RV Morphology and Function in Rats with PH Is Associated with Predominant Up-Regulation of mTORC1–S6

In contrast to simultaneous activation of mTORC1–S6 and mTORC2–Akt in pulmonary vasculature, RVs of rats with SuHx-induced PH 5 weeks after induction showed a roughly threefold increase in mTORC1-specific S6 phosphorylation rates, but only marginal elevation of mTORC2-specific P-S473 Akt, compared with controls (Figures 2A, 2B, and 2D), indicative of predominant activation of mTORC1 versus mTORC2 signaling. Supporting our observations, RVs from SuHx rats had a roughly twofold increase in phosphorylation rates of mTORC1 downstream effector, 4EBP1, without significant differences in mTORC2-specific P-SGK1 (6, 19) (Figures 2A, 2C, and 2E). Up-regulation of mTORC1–S6 pathway in PH RV was associated with significant cardiomyocyte and RV hypertrophy (assessed by cardiomyocyte cross-sectional area and Fulton index, respectively; Figures 3A–3C). Interestingly, rats with HPH, a less severe model of PH without marked endothelial involvement, although having significant elevation of sRVP and mPAP, RV hypertrophy, and RV contractility (max dP/dT; Figures E4A–E4D), had only moderate increases in both cardiomyocyte cross-sectional area and mTORC1-specific

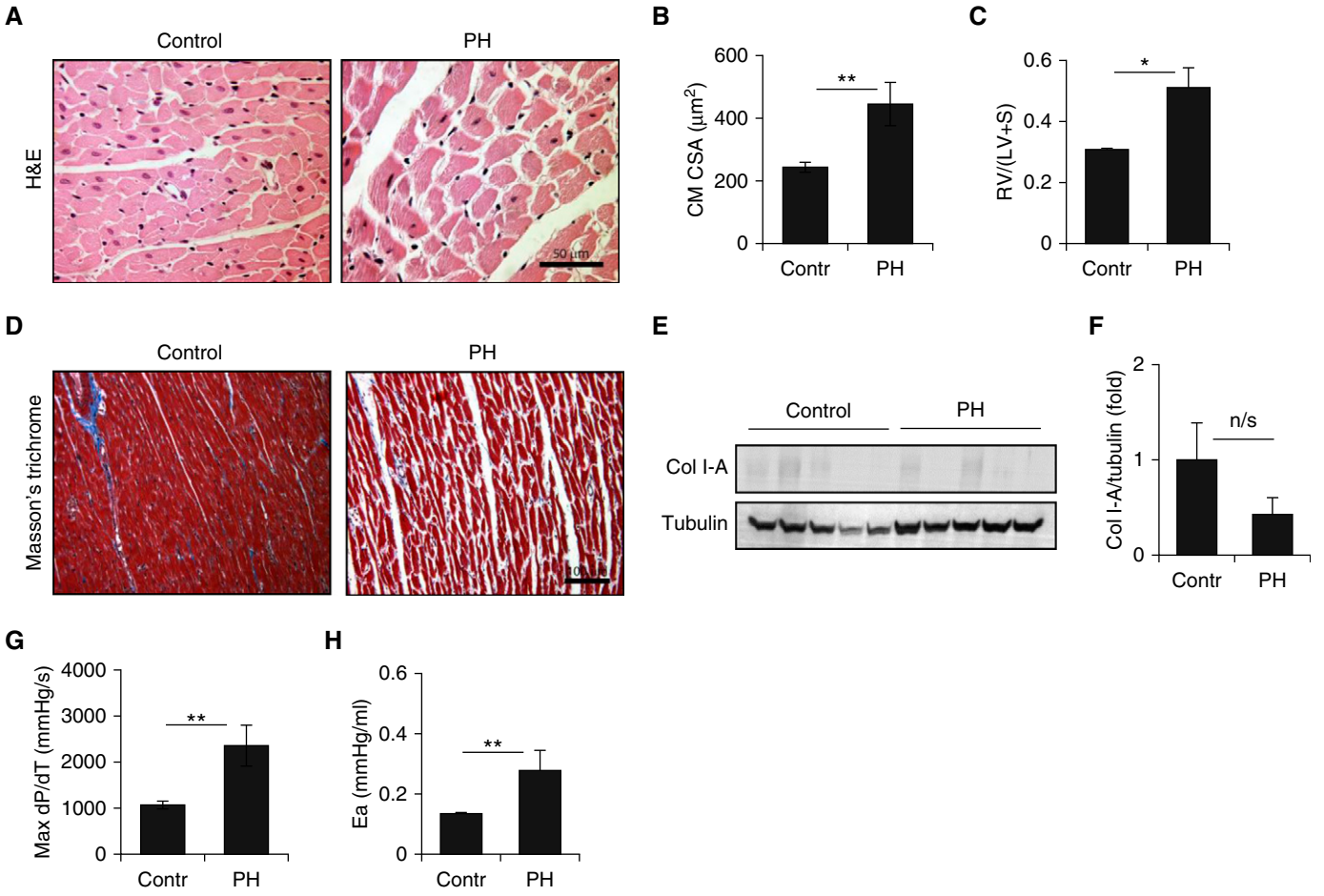

Figure 3. Impaired RV morphology and function in rats with SuHx-induced PH. (*A* and *B*) Representative images (*A*) and cardiomyocyte cross-sectional area (CM CSA) analysis (*B*) of RVs from male Sprague-Dawley rats with SuHx-induced PH (5 wk after induction) and age-matched controls. *Scale bar*: 50 μm. Data are means ± SE; $n = 5$–6 rats/group; 5 fields/animal, 12 cardiomyocytes/field were analyzed. $^{**}P < 0.05$. (*C*, *G*, and *H*) Fulton index (RV / [LV + S]), where LV is left ventricle and S is sputum (*C*), RV contractility (max dP/dT) (*G*), and arterial elastance (Ea) analyses (*H*) of rats with SuHx-induced PH (5 wk after induction) and age-matched controls; $n = 5$–6 animals/group; $^{*}P < 0.01$, $^{**}P < 0.05$. (*D–F*) Masson's trichrome staining (*D*) and immunoblot analysis (*E* and *F*) of RV tissues from rats with SuHx-induced PH (5 wk after induction) and age-matched controls. (*D*) Images are representative of five to six rats/group; minimum of six images/rat. *Scale bar*: 100 μm. (*F*) Data represent collagen I-A (Col I-A):tubulin ratio to control. Data are means ± SE; $n = 5$ rats/group.

S6 phosphorylation (Figures E3E–E3H). This confirms the link between the degree of mTORC1 activation and cardiomyocyte hypertrophy, and suggests a potential role of endothelial dysfunction in activation of mTORC1 signaling and cardiomyocyte hypertrophic response. Of note, we detected no increase in mTORC1–S6 or mTORC2–Akt signaling in LVs from either SuHx or HPH rats (Figures E4 and E5). Together, these data show that mTORC1–S6 up-regulation in PH is RV specific and is likely linked with RV cardiomyocyte hypertrophy.

SuHx rats had early stages of RV fibrosis (assessed by Masson's trichrome staining) without evident collagen I-A accumulation (Figures 3D–3F). Terminal hemodynamic analysis showed significant increase in max dP/dT and afterload (arterial elastance [Ea]) in the PH group compared with controls (Figures 3G and 3H), suggestive of adaptive/early-stage maladaptive RV response to hemodynamic stress at this stage of PH development. In support of terminal hemodynamic measurements, noninvasive echocardiography, performed on different groups of animals (groups 1 and 2, Figure E1) at the same time point (5 wk after PH induction) demonstrated marked increases in RV WT and RV:LV EDA ratio (with both significantly higher RV EDA and significantly lower LV EDA versus control), and shorter RV acceleration time compared with control rats (Figures 4, Figure E6).

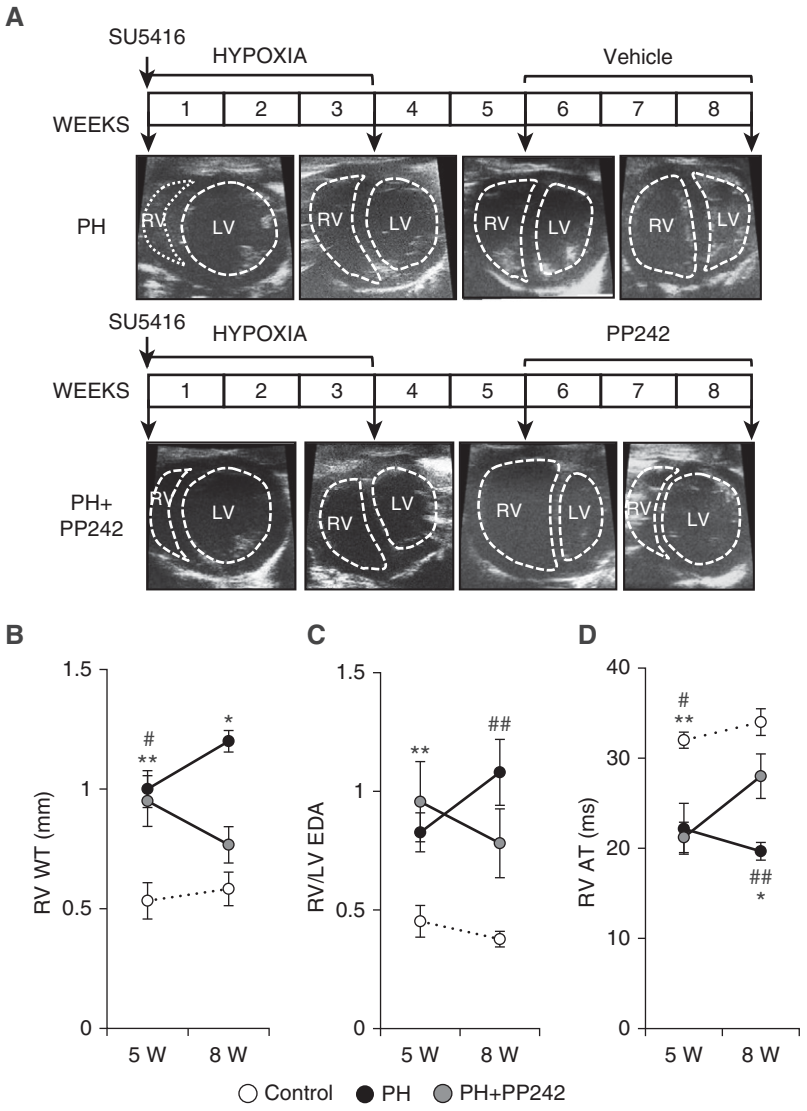

Figure 4. Effect of mTOR kinase inhibitor, PP242, on RV remodeling and acceleration time (AT) in rats with Su/Hx-induced PH. Repetitive, noninvasive echocardiography of rats with SuHx-induced PH treated with vehicle or PP242 at Weeks 6–8 after PH induction. Controls were age- and sex-matched rats maintained under normoxia. (*A*) Representative heart echocardiography images from six rats/group. *Dashed lines*, ventricles outlines. (*B–D*) RV wall thickness (WT) (*B*), RV:LV end-diastolic area (EDA) ratio (*C*), and RV-AT in control rats (*white circles*) and rats with SuHx-induced PH before and after treatment with vehicle (PH; *black circles*) and PP242 (PH + PP242, *gray circles*) (5 and 8 wk, respectively). Data are means ± SE; $n = 5$–6 rats/group. (*B*) $^{\#}P < 0.01$ for PH 5 weeks versus control 5 weeks; $^{**}P < 0.05$ for PH + PP242 5 weeks versus control 5 weeks; $^{*}P < 0.01$ for PH + PP242 8 weeks versus PH 8 weeks and for PH 8 weeks versus control. (*C*) $^{**}P < 0.05$ for PH 5 weeks versus control 5 weeks; PH + PP242 5 weeks versus control 5 weeks; $^{\#\#}P < 0.05$ for PH + PP242 8 weeks versus PH 8 weeks. (*D*) $^{\#}P < 0.01$ for control 5 weeks versus PH + PP242 5 weeks; $^{**}P < 0.05$ for control 5 weeks versus PH 5 weeks; $^{\#\#}P < 0.05$ for PH 8 weeks versus PH PP242 8 weeks; $^{*}P < 0.01$ for PH 8 weeks versus control 8 weeks.

PP242 Down-Regulates mTORC1–S6 and mTORC2–Akt in Small PAs, Reduces Established Pulmonary Vascular Remodeling and PH

To determine the effects of pharmacological inhibition of mTOR kinase on established pulmonary vascular remodeling and PH, rats with SuHx-induced PH were treated with vehicle or small ATP–competitive mTOR kinase inhibitor, PP242, (20 mg/kg, intraperitoneal, 5 d/wk) for 3 weeks starting at the beginning of Week 6 (Figure E1, groups 1 and 2, respectively). PP242-treated animals had marked decreases of both mTORC1–S6 and mTORC2–Akt pathways in SMA-positive areas of small PAs (Figures 5A and 5B) and significant decreases in PA medial thickness to the levels comparable to controls (Figures 5C and 5D), supporting our previous findings showing that PP242 inhibits human PAH PAVSMC proliferation and reverses VSM remodeling in rats with HPH (7).

In agreement with previously published studies (15, 16), vehicle-treated rats had neointimal vascular occlusion of small (20–50 μm outer diameter) PAs (detected by vWF staining) (Figures 5E and 5F, Figure E7). Importantly, PP242-treated rats had a significantly lower number of small PAs with full neointimal occlusion and higher numbers of nonoccluded vessels compared with the vehicle-treated group

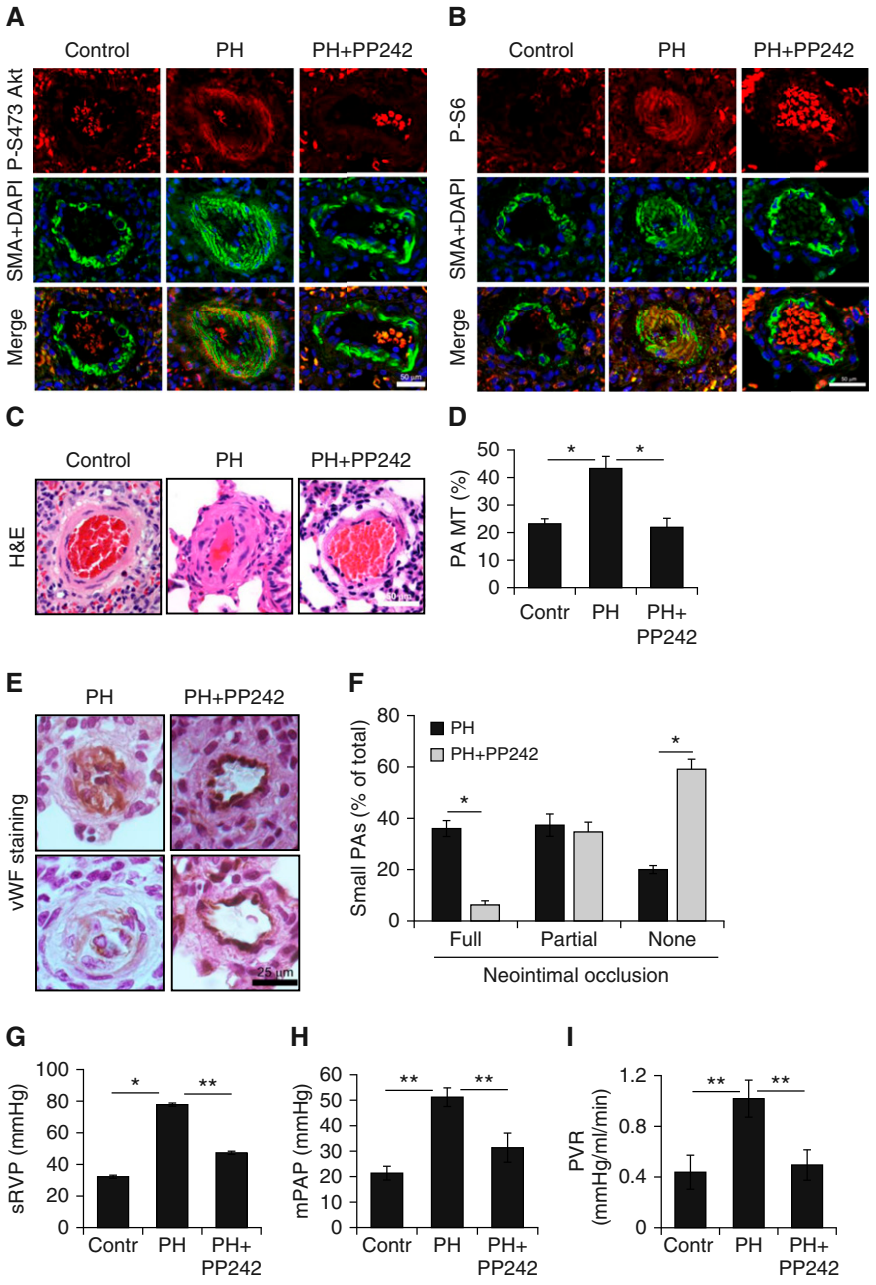

Figure 5. PP242 inhibits mTORC1–S6 and mTORC2–Akt in small PAs, reverses pulmonary vascular remodeling, and reduces pulmonary hypertension. (*A* and *B*) Immunohistochemical analysis of lung tissues from male Sprague–Dawley rats with SuHx-induced PH treated with vehicle or PP242 for 3 weeks starting at Week 6 after PH induction and age-matched controls to detect P-S6 (*red*, *A*), P-Akt (*red*, *B*), SMA (*green*) and DAPI (*blue*). *Yellow*: SMA (*green*) and P-S6 (*red*) or P-Akt (*red*, *B*) overlap. Images are representative of 3 animals per condition, minimum of 10 vessels per animal. *Scale bars*: 50 μm. (*C* and *D*) PA medial thickness (PA MT) analysis of rats treated as described above. Representative images of H&E-stained lung sections (*C*) and PA MT analysis (*D*). *Scale bar*: 50 μm; $n = 5$–6 rats/group; minimum of 10 PAs/rat. Data are means ± SE; $^{*}P < 0.01$. (*E* and *F*) Immunostaining with anti–von Willebrand factor (vWF) antibody (*brown*) performed on lung tissue sections of rats treated with vehicle or PP242 at Weeks 6–8 after PH induction. DAPI staining (*blue*) was performed to detect nuclei. *See* also Figure E7 for additional images. (*E*) Images are representative of five rats/group. *Scale bar*: 25 μm. (*F*) *Black bars*, PH + vehicle (PH); *gray bars*, PH + PP242. Data are means ± SE from $n = 5$ rats/group, 45 PAs/rat; $^{*}P < 0.001$. (*G–I*) sRVP (*G*), mPAP (*H*), and PVR (*I*) of rats treated as described above. Data are means ± SE; $n = 5$–6 animals/group; $^{*}P < 0.01$, $^{**}P < 0.05$. *See* also Figure E2 for systemic LV pressure and mean arterial pressure measurements.

(Figures 5E and 5F, Figure E7), showing that, in addition to inhibiting PAVSMC proliferation, PP242 also prevents neointimal PAEC overgrowth. To confirm our findings, we tested the effect of PP242 on human distal PAECs from subjects with PAH. Similar to a previously published study (18), PAH PAECs showed increased growth in culture compared with nondiseased (control) cells (Figure E8A). Importantly, PP242 inhibited both mTORC1-specific P-S6 and mTORC2-specific P-S473 Akt, and reduced PAH PAEC growth in a concentration-dependent manner (Figures E8B–E8E).

Terminal hemodynamic analysis demonstrated significantly lower sRVP, mPAP, and PVR in PP242-treated SuHx rats compared with vehicle-treated animals (Figures 5G–5I). No significant differences have been detected in systemic LV pressure and mean arterial pressure among control, vehicle-treated PH, and PP242-treated PH groups (Figure E9). Taken together, these data demonstrate that PP242 inhibits mTORC1–S6 and mTORC2–Akt and VSM remodeling, attenuates PAEC growth and neointimal vascular occlusion of small PAs, reverses pulmonary vascular remodeling, and reduces established PH.

PP242 Down-Regulates mTORC1–S6, but Not mTORC2–Akt, in PH RV, Reverses RV Remodeling, Improves RV Functional Outcomes, and Prevents RV Fibrosis

Immunoblot analysis of RVs from vehicle-treated rats showed further increase in mTORC1-specific S6 phosphorylation rates without marked changes in mTORC2-specific P-S473 compared with controls (Figures 6A–6C), confirming predominant dysregulation of mTORC1 versus mTORC2 signaling in RV during PH progression. Importantly, 3 weeks of PP242 treatment down-regulated mTORC1–S6 without affecting basal mTORC2–Akt, as shown by decreases in S6 phosphorylation, but preserved P-S473 Akt phosphorylation rates (Figures 6A–6C). Vehicle-treated rats had profound cardiomyocyte and RV hypertrophy that were significantly decreased in the PP242-treated group (Figures 6D–6F). Interestingly, RVs of vehicle-treated rats had extensive fibrosis and significant increases in collagen I-A accumulation (Figures 6G–6I). In contrast, RVs of PP242-treated animals showed no evidence of fibrosis, and had collagen I-A

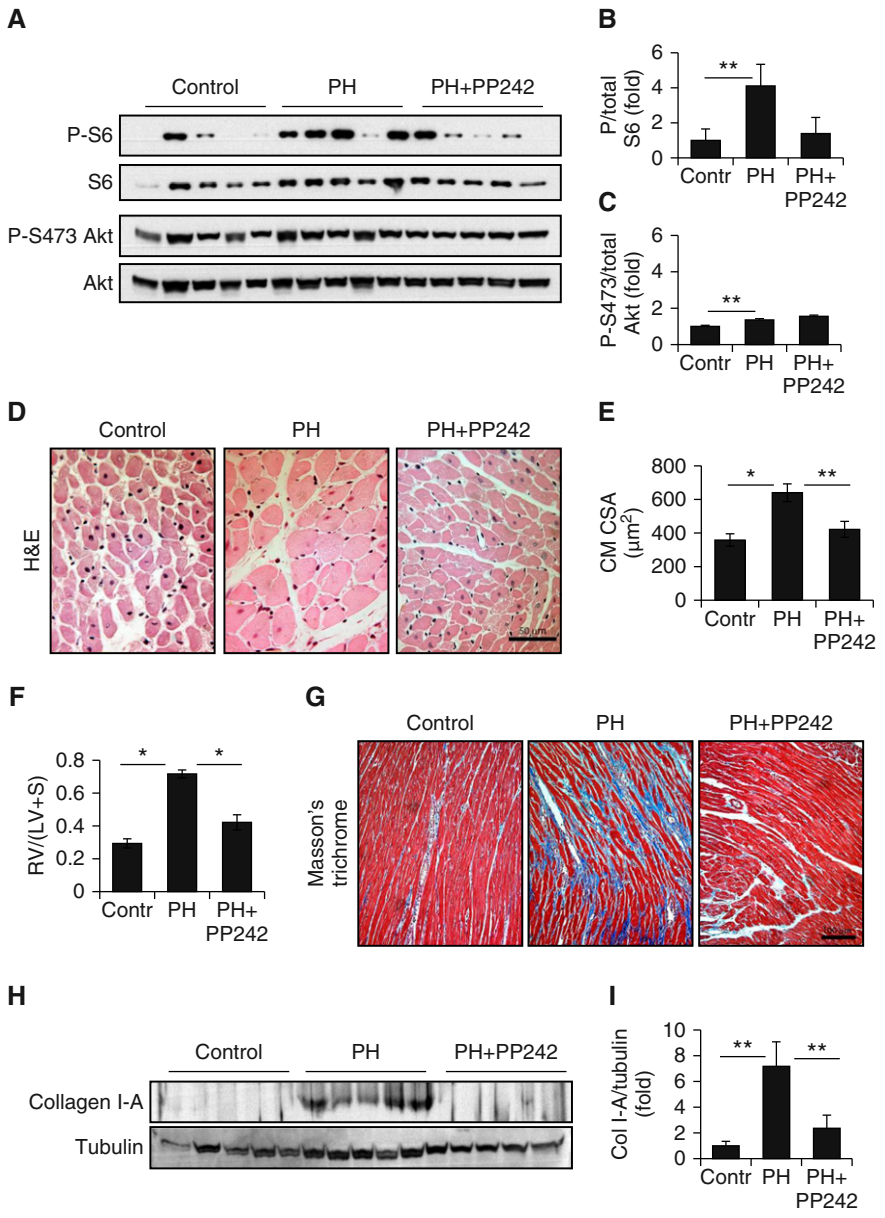

Figure 6. PP242 reduces mTORC1–S6, but not mTORC2–Akt, decreases cardiomyocytes hypertrophy, and prevents fibrosis in RVs from rats with SuHx PH. Rats with SuHx-induced PH were treated with vehicle (PH group) or PP242 (PH + PP242 group) at Weeks 6–8 after PH induction; RVs were collected for immunoblot, morphological, and histochemical analyses. Controls are age- and sex-matched rats maintained under normoxia. (*A–C*) Immunoblot analysis of RV tissues to detect indicated proteins. Data are fold changes in p/total protein ratio to controls; $n = 5$ animals/group; $^{**}P < 0.05$. (*D* and *E*) Analysis of cardiomyocyte cross-sectional areas (CM CSA). Representative images (*D*) and statistical analysis (*E*) of H&E-stained RV sections from 6 rats/group, 6 random images/rat, 12 randomly selected cardiomyocytes/image analyzed. *Scale bar*: 50 μm. Data are means ± SE; $^{*}P < 0.01$; $^{**}P < 0.05$. (*F*) Fulton index was calculated as a RV / (LV + S) ratio; $n = 5$–6 rats/group; $^{*}P < 0.01$. (*G*) Representative images of Masson's trichrome staining from five to six rats/group; minimum of six images/rat. *Scale bar*: 100 μm. (*H* and *I*) Immunoblot analysis of RV tissues to detect collagen I-A and tubulin. Data are fold changes in collagen I-A (Col I-A):tubulin ratio to control; $n = 5$ animals/group; $^{**}P < 0.05$.

levels similar to those in the control group (Figures 6G–6I), demonstrating that PP242 treatment protects from the development of RV fibrosis. Noninvasive echocardiography showed morphological and functional RV worsening in vehicle-treated rats, as detected by further thickening of RV wall, increase in RV:LV EDA ratio, and decline in RV acceleration time compared with the 5-week time point (Figures 4, Figure E6). Terminal hemodynamic analysis, performed after noninvasive measurements, demonstrated a further increase in max dP/dT and Ea (Figures 7A and 7B), also supporting RV functional impairment. Importantly, PP242 reduced RV WT and RV:LV EDA ratio, improved RV AT (Figures 4, Figure E6), and significantly reduced max dP/dT and Ea to levels similar to those in the control group (Figures 7A and 7B). In aggregate, these data demonstrate that mTOR kinase inhibitor, PP242, down-regulates RV-specific mTORC1–S6 activation, reverses RV remodeling, improves RV functional outcomes, and prevents development of RV fibrosis.

Interestingly, there was significant linear correlation between sRVP and RV:LV EDA ratio levels (data not shown), suggesting that the observed RV changes are largely attributable to the changes in sRVP. To test whether RV-specific mTORC1–S6 activation is fully pressure dependent, we performed short-term (3 d) PP242 treatment of SuHx-exposed rats at 8 weeks after PH initiation (Figure E2). As expected, we found no significant changes in sRVP, mPAP, or RV hypertrophy between the vehicle- and PP242-treated groups (Figures E10A–E10C). Interestingly, RVs from PP242-treated rats also showed no significant differences in mTORC1-specific P-S6, mTORC2-specific P-S473 Akt, and contractility (Figures E10D–E10G). Although further studies are needed, these data strongly suggest that positive effects of PP242 on RV-specific mTORC1 signaling, RV morphology, and function are predominantly due to a PP242-induced reduction of PAP and a decrease in RV afterload.

Discussion

mTOR is a key regulator of cell growth, proliferation, and survival, and its dysregulation plays an important role in multiple pathological conditions (20, 21), including pulmonary vascular remodeling in PAH (6, 22). The existence of two functionally distinct complexes, growth-promoting mTORC1 and prosurvival mTORC2, led us to speculate that mTOR may play different roles in different organs, depending on the status of each complex activation. Here, we report that there are

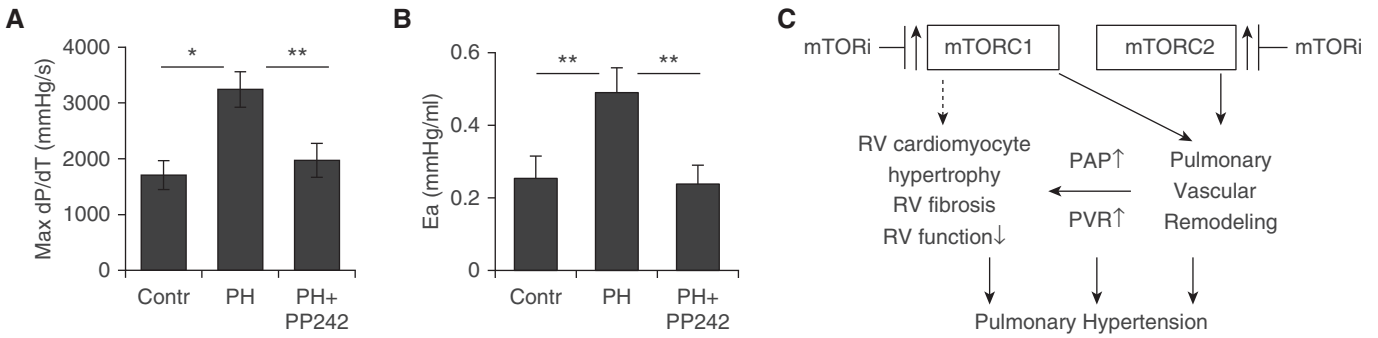

Figure 7. (*A* and *B*) PP242 improves RV functional outcomes. RV contractility (max dP/dT) and afterload (Ea) analyses of rats with SuHx-induced PH treated with vehicle (PH group) or PP242 (PH + PP242 group) at Weeks 6–8 after PH induction and age- and sex-matched controls; $n = 5$–6 animals/group; $^{*}P < 0.01$, $^{**}P < 0.05$. (*C*) Schematic representation of the relative roles of mTORC1 and mTORC2 pathways in pulmonary hypertension based on our previous (7) and current findings. Both mTORC1 and mTORC2 pathways are activated in small remodeled PAs and are required for pulmonary vascular remodeling; predominantly mTORC1 signaling is activated in RV, which promotes cardiomyocyte hypertrophy and RV fibrosis. Dual mTORC1/mTORC2 inhibition with mTOR inhibitor (mTORi), PP242, inhibits mTORC1/mTORC2 activation in small PAs and mTORC1 signaling in RV, reverses pulmonary vascular remodeling and RV hypertrophy, prevents RV fibrosis, improves RV functional outcomes, and reduces overall PH.

different patterns of mTORC1 versus mTORC2 activation in pulmonary vasculature and RV in rats with SuHx-induced PH. In contrast to simultaneous up-regulation of both mTORC1 and mTORC2 pathways in small remodeled PAs, RVs, but not LVs, from PH rats had robust activation of mTORC1 signaling, but only mediocre increases in mTORC2–Akt (Figure 7C), suggestive of a predominant role of mTORC1 versus mTORC2 in RV dysfunction.

The mTORC1 signaling is a master regulator of protein, lipid, and nucleotide synthesis, up-regulation of which induces cell growth and hypertrophic response (21, 23). mTORC1 activation appeared to be a key signaling event promoting volume and pressure overload–induced LV hypertrophy and fibrosis, and is currently considered as a potentially highly attractive molecular target to treat human disorders associated with pathological cardiac hypertrophy and cardiomyopathy (21). We found that persistent RV-specific activation of mTORC1 pathway in rats with SuHx-induced PH was associated with progressive cardiomyocyte hypertrophy that was accompanied by profound fibrosis as PH progressed. The morphological changes were paralleled by dysregulation of RV functional parameters, suggestive of involvement of mTORC1 in both early adaptive and late maladaptive RV responses to chronic pressure overload.

Interestingly, in contrast to microvascular PAVSMCs, RVs from PH rats had only marginal increases in mTORC2–Akt that did not elevate with PH progression. Pharmacological inhibition of mTOR with small ATP–competitive inhibitor, PP242, while suppressing both mTORC1–S6 and mTORC2–Akt in pulmonary vasculature, in right heart reduced only mTORC1–S6 without affecting basal mTORC2–Akt signaling. Of note, the mTORC2–Akt pathway, which plays a pathological role in PAH pulmonary vascular remodeling by supporting survival of proliferative, apoptosis-resistant PAVSMCs (7, 24), also acts as a cardioprotector via preserving cardiomyocytes' survival (25–27), and may be of benefit to sustaining protection of cardiomyocytes from apoptosis.

We previously demonstrated that dual mTORC1/mTORC2 inhibition by PP242 selectively promotes PAH PAVSMC apoptosis and reverses established pulmonary vascular remodeling (7). Here, we report that, in addition to targeting PAVSMC, PP242 also markedly reduces the number of pulmonary arterioles with neointimal occlusion in rats with SuHx-induced PH, and significantly inhibits growth of PAECs from human PAH lungs, showing the benefits of PP242 treatment in targeting both PAVSMC and PAEC hyperproliferation in PAH. Together with observed differences in mTOR signaling between pulmonary vasculature and RV, these findings now raise the possibility that small ATP–competitive mTOR kinase inhibitors can be used to simultaneously reverse pulmonary vascular remodeling and improve, or at least not worsen, RV morphology and function. Indeed, we found that treatment of rats with established PH with PP242 not only reversed pulmonary vascular remodeling and markedly reduced PAP and PVR, but also reversed RV remodeling and improved RV functional outcomes.

Importantly, PP242-dependent inhibition of mTORC1 not only reversed cardiomyocytes and overall PH hypertrophy, but also improved RV function and prevented progression of RV fibrosis and collagen I-A accumulation. This antifibrotic effect of mTORC1 inhibition, together with its ability to normalize RV size via reversing cardiomyocyte hypertrophy, is suggestive of benefits of mTORC1 inhibitors in preventing or attenuating maladaptive RV remodeling. It is possible, however, that the benefits of mTORC1 inhibition may be broader than halting RV hypertrophy and fibrosis. mTORC1 is a metabolic regulator, and its activation enhances glycolysis and inhibits autophagy (21). Although not linked with up-regulation of mTORC1, the metabolic shift to glycolysis and impaired autophagic flux has been reported, and plays important roles in RV dysfunction in human PAH and experimental PH (28–30). Further studies are required to determine whether mTORC1 inhibition would be beneficial to correct RV metabolic abnormalities and impaired autophagic response.

Our study suggests that such selectivity of PP242 toward mTORC1–S6 in remodeled RVs may be explained by its indirect positive effect on right heart via reducing PAP and RV afterload, and the potential benefits of direct mTORC1 inhibition in RV remain to be determined. Interestingly, phosphodiesterase type 5

inhibitors, which act, at least in part, via inhibition of mTORC1–S6K1 signaling in cancer cells (31, 32), also demonstrated both antiremodeling and heart-protecting effects in experimental PH as single agents or in combination with other PH-focused therapies. Thus, phosphodiesterase type 5 inhibitor, sildenafil, prevented RV hypertrophy and RV failure in rats with monocrotaline-induced PH (33). In addition, tadalafil, although having a modest effect as a monotherapy, synergized with the type A endothelin receptor antagonist, ambrisentan, in reversing pulmonary hemodynamic impairment, RV hypertrophy, and RV functional deficit in the SuHx rat model (34).

Collectively, our study demonstrates that there are different patterns of mTORC activation in pulmonary hypertensive pulmonary vasculature and RV with up-regulation of both mTORC1–S6 and mTORC2–Akt pathways in small remodeled PAs, and predominant activation of mTORC1–S6 in remodeled RV. We also show that pharmacological inhibition of mTOR kinase activity reverses pulmonary vascular remodeling, reduces PH, and improves RV morphology and function (Figure 7C). The attractiveness of mTOR kinase inhibitors as a potential therapeutic option is further supported by our observation that PP242 targets both mTORC1 and mTORC2 in pulmonary vasculature, but only mTORC1 in RV, preserving basal mTORC2–Akt levels, which may be beneficial for cardiomyocytes' survival.

We recognize that our study has limitations associated with the lack of data on the status of mTOR signaling in human PAH RVs that arise from the nature of the studied disease. PAH is a rare disease with extremely poor availability of human RV tissue for research of this type. However, given our current and previous findings (7), and the fact that mTOR kinase inhibitors exhibited tolerable and manageable toxicity in phase I, and reached phase II clinical trials for treatment of various cancers (35), the potential beneficial effects of mTOR kinase inhibitors on human RV pathology in other models of experimental PH are worthy of further investigation. ■

Author disclosures are available with the text of this article at www.atsjournals.org.

References

1. Humbert M, Morrell NW, Archer SL, Stenmark KR, MacLean MR, Lang IM, Christman BW, Weir EK, Eickelberg O, Voelkel NF, *et al*. Cellular and molecular pathobiology of pulmonary arterial hypertension. *J Am Coll Cardiol* 2004;43(12 suppl S):13S–24S.
2. Tuder RM, Archer SL, Dorfmüller P, Erzurum SC, Guignabert C, Michelakis E, Rabinovitch M, Schermuly R, Stenmark KR, Morrell NW. Relevant issues in the pathology and pathobiology of pulmonary hypertension. *J Am Coll Cardiol* 2013; 62(25 suppl): D4–D12.
3. Morrell NW, Archer SL, Defelice A, Evans S, Fiszman M, Martin T, Saulnier M, Rabinovitch M, Schermuly R, Stewart D, *et al*. Anticipated classes of new medications and molecular targets for pulmonary arterial hypertension. *Pulm Circ* 2013;3:226–244.
4. Yeh ETH, Tong AT, Lenihan DJ, Yusuf SW, Swafford J, Champion C, Durand J-B, Gibbs H, Zafarmand AA, Ewer MS. Cardiovascular complications of cancer therapy: diagnosis, pathogenesis, and management. *Circulation* 2004;109:3122–3131.
5. Laplante M, Sabatini DM. mTOR signaling at a glance. *J Cell Sci* 2009; 122:3589–3594.
6. Goncharova EA. mTOR and vascular remodeling in lung diseases: current challenges and therapeutic prospects. *FASEB J* 2013;27: 1796–1807.
7. Goncharov DA, Kudryashova TV, Ziai H, Ihida-Stansbury K, DeLisser H, Krymskaya VP, Tuder RM, Kawut SM, Goncharova EA. Mammalian target of rapamycin complex 2 (mTORC2) coordinates pulmonary artery smooth muscle cell metabolism, proliferation, and survival in pulmonary arterial hypertension. *Circulation* 2014;129:864–874.
8. Houssaini A, Abid S, Mouraret N, Wan F, Rideau D, Saker M, Marcos E, Tissot C-M, Dubois-Randé J-L, Amsellem V, *et al*. Rapamycin reverses pulmonary artery smooth muscle cell proliferation in pulmonary hypertension. *Am J Respir Cell Mol Biol* 2013;48:568–577.
9. Krymskaya VP, Snow J, Cesarone G, Khavin I, Goncharov DA, Lim PN, Veasey SC, Ihida-Stansbury K, Jones PL, Goncharova EA. mTOR is required for pulmonary arterial vascular smooth muscle cell proliferation under chronic hypoxia. *FASEB J* 2011:25: 1922–1933.
10. Aghamohammadzadeh R, Zhang Y-Y, Stephens TE, Arons E, Zaman P, Polach KJ, Matar M, Yung L-M, Yu PB, Bowman FP, *et al*. Up-regulation of the mammalian target of rapamycin complex 1 subunit Raptor by aldosterone induces abnormal pulmonary artery smooth muscle cell survival patterns to promote pulmonary arterial hypertension. *FASEB J* 2016;30:2511–2527.
11. Kudryashova TV, Goncharov DA, Pena A, Ihida-Stansbury K, DeLisser H, Kawut SM, Goncharova EA. Profiling the role of mammalian target of rapamycin in the vascular smooth muscle metabolome in pulmonary arterial hypertension. *Pulm Circ* 2015;5:667–680.
12. Taraseviciene-Stewart L, Kasahara Y, Alger L, Hirth P, Mc Mahon G, Waltenberger J, Voelkel NF, Tuder RM. Inhibition of the VEGF receptor 2 combined with chronic hypoxia causes cell death–dependent pulmonary endothelial cell proliferation and severe pulmonary hypertension. *FASEB J* 2001;15:427–438.
13. Kudryashova TV, Goncharov DA, Pena A, Kelly N, Vanderpool R, Baust J, Kobir A, Shufesky W, Mora AL, Morelli AE, *et al*. HIPPO–integrin–linked kinase cross-talk controls self-sustaining proliferation and survival in pulmonary hypertension. *Am J Respir Crit Care Med* 2016;194:866–877.
14. Alzoubi A, Toba M, Abe K, O'Neill KD, Rocic P, Fagan KA, McMurtry IF, Oka M. Dehydroepiandrosterone restores right ventricular structure and function in rats with severe pulmonary arterial hypertension. *Am J Physiol Heart Circ Physiol* 2013;304: H1708–H1718.
15. Abe K, Toba M, Alzoubi A, Ito M, Fagan KA, Cool CD, Voelkel NF, McMurtry IF, Oka M. Formation of plexiform lesions in experimental severe pulmonary arterial hypertension. *Circulation* 2010;121: 2747–2754.
16. Toba M, Alzoubi A, O'Neill KD, Gairhe S, Matsumoto Y, Oshima K, Abe K, Oka M, McMurtry IF. Temporal hemodynamic and histological progression in Sugen5416/hypoxia/normoxia-exposed pulmonary arterial hypertensive rats. *Am J Physiol Heart Circ Physiol* 2014;306: H243–H250.
17. Kasimir M-T, Seebacher G, Jaksch P, Winkler G, Schmid K, Marta GM, Simon P, Klepetko W. Reverse cardiac remodelling in patients with primary pulmonary hypertension after isolated lung transplantation. *Eur J Cardiothorac Surg* 2004;26:776–781.
18. Masri FA, Xu W, Comhair SAA, Asosingh K, Koo M, Vasanji A, Drazba J, Anand-Apte B, Erzurum SC. Hyperproliferative apoptosis-resistant endothelial cells in idiopathic pulmonary arterial hypertension. *Am J Physiol Lung Cell Mol Physiol* 2007;293:L548–L554.
19. Heikamp EB, Patel CH, Collins S, Waickman A, Oh M-H, Sun I-H, Illei P, Sharma A, Naray-Fejes-Toth A, Fejes-Toth G, *et al*. The AGC kinase SGK1 regulates TH1 and TH2 differentiation downstream of the mTORC2 complex. *Nat Immunol* 2014;15:457–464.
20. Zoncu R, Efeyan A, Sabatini DM. mTOR: from growth signal integration to cancer, diabetes and ageing. *Nat Rev Mol Cell Biol* 2011;12: 21–35.
21. Sciarretta S, Volpe M, Sadoshima J. Mammalian target of rapamycin signaling in cardiac physiology and disease. *Circ Res* 2014;114: 549–564.

22. Pullamsetti SS, Savai R, Seeger W, Goncharova EA. From cancer biology to new PAH therapeutics: targeting cell growth and proliferation signaling hubs. *Am J Respir Crit Care Med* 2017;195: 425–437.
23. Taneike M, Nishida K, Omiya S, Zarrinpashneh E, Misaka T, Kitazume-Taneike R, Austin R, Takaoka M, Yamaguchi O, Gambello MJ, *et al*. mTOR hyperactivation by ablation of tuberous sclerosis complex 2 in the mouse heart induces cardiac dysfunction with the increased number of small mitochondria mediated through the down-regulation of autophagy. *PLoS One* 2016;11:e0152628.
24. Tang H, Chen J, Fraidenburg DR, Song S, Sysol JR, Drennan AR, Offermanns S, Ye RD, Bonini MG, Minshall RD, *et al*. Deficiency of Akt1, but not Akt2, attenuates the development of pulmonary hypertension. *Am J Physiol Lung Cell Mol Physiol* 2015;308:L208–L220.
25. Sciarretta S, Zhai P, Maejima Y, Del Re DP, Nagarajan N, Yee D, Liu T, Magnuson MA, Volpe M, Frati G, *et al*. mTORC2 regulates cardiac response to stress by inhibiting MST1. *Cell Reports* 2015;11:125–136.
26. Yano T, Ferlito M, Aponte A, Kuno A, Miura T, Murphy E, Steenbergen C. Pivotal role of mTORC2 and involvement of ribosomal protein S6 in cardioprotective signaling. *Circ Res* 2014;114:1268–1280.
27. Völkers M, Konstandin MH, Doroudgar S, Toko H, Quijada P, Din S, Joyo A, Ornelas L, Samse K, Thuerauf DJ, *et al*. Mechanistic target of rapamycin complex 2 protects the heart from ischemic damage. *Circulation* 2013;128:2132–2144.
28. Katz WE, Gasior TA, Quinlan JJ, Lazar JM, Firestone L, Griffith BP, Gorcsan J III. Immediate effects of lung transplantation on right ventricular morphology and function in patients with variable degrees of pulmonary hypertension. *J Am Coll Cardiol* 1996;27:384–391.
29. Habedank D, Ewert R, Hummel M, Dandel M, Habedank F, Knosalla C, Lehmkuhl HB, Anker SD, Hetzer R. The effects of bilateral lung transplantation on ventilatory efficiency, oxygen uptake and the right heart: a two-yr follow-up. *Clin Transplant* 2011;25:E38–E45.
30. Ryan JJ, Huston J, Kutty S, Hatton ND, Bowman L, Tian L, Herr JE, Johri AM, Archer SL. Right ventricular adaptation and failure in pulmonary arterial hypertension. *Can J Cardiol* 2015;31:391–406.
31. Booth L, Roberts JL, Cruickshanks N, Tavallai S, Webb T, Samuel P, Conley A, Binion B, Young HF, Poklepovic A, *et al*. PDE5 inhibitors enhance celecoxib killing in multiple tumor types. *J Cell Physiol* 2015;230:1115–1127.
32. Tavallai M, Hamed HA, Roberts JL, Cruickshanks N, Chuckalovcak J, Poklepovic A, Booth L, Dent P. Nexavar/Stivarga and viagra interact to kill tumor cells. *J Cell Physiol* 2015;230:2281–2298.
33. Xie Y-P, Chen B, Sanders P, Guo A, Li Y, Zimmerman K, Wang L-C, Weiss RM, Grumbach IM, Anderson ME, *et al*. Sildenafil prevents and reverses transverse-tubule remodeling and Ca(2+) handling dysfunction in right ventricle failure induced by pulmonary artery hypertension. *Hypertension* 2012;59:355–362.
34. Cavasin MA, Demos-Davies KM, Schuetze KB, Blakeslee WW, Stratton MS, Tuder RM, McKinsey TA. Reversal of severe angioproliferative pulmonary arterial hypertension and right ventricular hypertrophy by combined phosphodiesterase-5 and endothelin receptor inhibition. *J Transl Med* 2014;12:314.
35. Zheng Y, Jiang Y. mTOR Inhibitors at a glance. *Mol Cell Pharmacol* 2015;7:15–20.